A Comparative Study of Collision-Induced and Surface-Induced Dissociation. 1. Fragmentation of Protonated Dialanine

Julia Laskin,* Eduard Denisov, and Jean Futrell

Contribution from the Pacific Northwest National Laboratory, William R. Wiley Environmental Molecular Sciences Laboratory, P.O. Box 999 (K8-96), Richland, Washington 99352

Received April 20, 2000

Abstract: Collision-induced and surface-induced dissociation of protonated dialanine (Ala-AlaH$^+$) was studied using a 7 T Fourier Transform Ion Cyclotron Resonance Mass Spectrometer (FT-ICR MS). Energy-resolved fragmentation efficiency curves were obtained using both techniques. The results were modeled using RRKM/QET formalism. The energetics and dynamics of the four primary and some secondary fragmentation pathways were determined from the RRKM modeling. Both multiple-collision CID and SID results could be reproduced within the same model. The strong correspondence of fragmentation efficiency curves obtained in the high-pressure CID and SID experiments indicates that the internal energy distributions of Ala-AlaH$^+$ activated by multiple collisions and by surface impact are remarkably similar.

Introduction

Tandem mass spectrometry (MS/MS) continues to play an important role in basic research of gas-phase ion chemistry and ion structure determination. With the advent of soft ionization techniques such as electrospray (ESI)[1] and matrix-assisted laser desorption ionization (MALDI),[2] tandem mass spectrometry became a very useful tool for peptide sequencing, structure determination, and investigation of the fragmentation mechanisms of biomolecules. MS/MS experiments involve mass selection of the ion of interest in the first MS stage, excitation of the ion followed by its dissociation, and mass analysis of the resulting fragments in the second MS stage. A wide variety of mass filters and ion excitation methods can be employed in these experiments, making tandem mass spectrometry an extremely flexible analytical technique that can be implemented on almost any type of mass spectrometer. The progress in application of MS/MS to large molecules is summarized in several recent reviews.[3−7]

Collisional activation (CA) is one of the most commonly used excitation methods in MS/MS experiments. Both basic principles of CA and various aspects of its application to polyatomic ions have been extensively discussed in several recent reviews.[4,8−10] Traditionally excitation of the precursor ion was achieved by high-energy collisions with neutral gas where the probability for multiple collisions to occur is relatively low. Single-collision CA was extensively used to study fragmentation of small and medium-size molecules. However, with increasing size of the ion its dissociation rate decreases dramatically, implying that very high internal energy has to be deposited into the ion to induce fragmentation on the time scale of the experiment. Moreover, center-of-mass (CM) collision energy and, consequently, the maximum energy available for CA decreases with increase in ion mass. As a result, it becomes difficult to induce dissociation of large ions using conventional single-collision activation. These limitations can be readily overcome by using low-energy multiple-collision activation or, alternatively, replacing a gas molecule with surface. Surface-induced dissociation (SID)[11−13] and multiple-collision activation (MCA-CID)[5] have proven to be effective methods for the activation and dissociation of large molecules. However, little quantitative information on similarities and differences between these activation techniques is available thus far. Fragmentation patterns of ions activated using either of these methods will depend on the internal energy distribution of excited ions (energy deposition function, EDF) and the reaction time sampled in the experiment. While the reaction time can be easily estimated based on the individual experimental setup, determination of the energy deposition function remains challenging.

Several indirect methods for determining EDF have been proposed. A probability theory-based method has been developed by Kim[14] for high-energy tandem mass spectrometry CID to account for the effects of sequential collisional excitation in a small number of collisions. An analytical expression for the collisional EDF for high-energy collisions was derived based on the analysis of pressure dependence of the CID of methane.[15] Cooks and co-workers developed a "thermometer" ion method that can be applied to a system of consecutive reactions with

* Address correspondence to this author. E-mail: Julia.Laskin@pnl.gov. FAX: (509) 3763650.

(1) Fenn, J. B.; Mann, M.; Meng, C. K.; Wong, S. F.; Whitehouse, C. M. *Science* **1989**, *246*, 64.
(2) Hillenkamp, F.; Karas, M.; Beavis, R. C.; Chait, B. T. *Anal. Chem.* **1991**, *63*, 1193A.
(3) Senko, M. W.; Speir, J. P.; McLafferty, F. W. *Acc. Chem. Res.* **1994**, *66*, 2801.
(4) Marzluff, E. M.; Beauchamp, J. L. In *Large Ions: Their Vaporization, Detection and Structural Analysis*; Baer, T., Ng, C. Y., Powis, I.; Eds.; John Wiley & Sons Ltd.: New York, 1996.
(5) McLuckey, S. A.; Goeringer, D. E. *J. Mass Spectrom.* **1997**, *32*, 461.
(6) Williams, E. R. *Anal. Chem.* **1998**, *70*, 179A.
(7) Yates, J. R., III *J. Mass Spectrom.* **1998**, *33*, 1.
(8) Shukla, A. K.; Futrell, J. H. *Mass Spectrom. Rev.* **1993**, *12*, 211.
(9) McLuckey, S. A. *J. Am. Soc. Mass Spectrom.* **1992**, *3*, 599.
(10) Hayes, R. N.; Gross, M. L. *Methods Enzymol.* **1990**, *193*, 237.
(11) Cooks, R. G.; Ast, T.; Mabud, A. *Int. J. Mass Spectrom. Ion Processes* **1990**, *100*, 209.
(12) Cooks, R. G.; Ast T.; Pradeep T.; Wysocki V. *Acc. Chem. Res.* **1994**, *27*, 316.
(13) Dongré, A. R.; Somogyi, Á.; Wysocki,V. H. *J. Mass Spectrom.* **1996**, *31*, 339.
(14) Kim, M. S. *Int. J. Mass Spectrom. Ion Phys.***1983**, 50, 189.
(15) Lee, S. H.; Kim, M. S.; Beynon, J. H. *Int. J. Mass Spectrom. Ion Processes* **1987**, *75*, 83.

10.1021/ja001384w
Published on Web 09/23/2000

known endothermicities and similar entropy requirements.[16] The relative abundance of each fragment ion is taken as a measure of the number of ions produced with internal energies lying in the energy range where that particular fragment ion is dominant (the underlying assumption is that only one fragment is present in each energy range). This method has been used to compare internal energy distributions of molecular ions of transition metal carbonyls activated using different excitation approaches. The thermometer ion method gives only a relatively crude estimate for the EDF and is limited to ions that undergo consecutive fragmentation. An improved method (usually called "deconvolution" method) was introduced by Vékey et al. to determine the internal energy content of fragment ions produced by electron capture collisions and overcome certain limitations of the thermometer ion method.[17] In the deconvolution method the relative abundance of fragment ions is adopted from the experimentally measured fragmentation probabilities (breakdown curves). This method was used to determine the EDF of benzene ions excited by collisions with self-assembled monolayer (SAM) surfaces.[18] However, the requirement of the accurate knowledge of breakdown curves of an ion is a severe limitation of this approach.

Internal energy distributions obtained using these methods revealed that a relatively high percentage of kinetic energy (T) is converted to internal energy (E) upon SID and that SID produces ions with a much narrower spread of internal energies than does CID. The Recursive Internal Energy Distribution Search (REIDS) method was introduced by us and has been used to determine EDF of Cr $(CO)_6^{+\bullet}$ upon collisions with fluorinated SAM surface in FT-ICR.[19] This approach requires the knowledge of breakdown curves F(E) and an initial guess of the internal energy distribution, P(E). The intensity of a particular ion, i, in the mass spectrum is calculated as an integrated product of P(E) and $F_i(E)$. The whole mass spectrum is reconstructed by minimizing the squared residuals between the calculated and experimental mass spectra. The kinetic-to-internal energy conversion (T → V) was shown to rise with SID collision energy and reach a maximum of ca. 19% at 23 eV collision energy for Cr $(CO)_6^{+\bullet}$ collisions with fluorinated SAM surface.

Several theoretical studies addressed the efficiency of energy transfer upon CA and surface impact. Marzluff et al. used classical trajectory simulations to study collisional energy transfer for collisions of deprotonated Gly-Gly-Ile with nitrogen.[20] They have shown that on average 41% of the relative kinetic energy is transferred into internal modes of the peptide. Energy conversion of greater than 90% at a relative collision energy of 100 eV was predicted for collisions of protonated bradykinin with nitrogen. The high efficiency of energy transfer was attributed to multiple interactions between the ion and the neutral encounter.[4] Meroueh and Hase[21] conducted a thorough investigation of collisional activation of polyglycines as a function of impact parameter, peptide size, and structure. According to these simulations in the low collision energy regime, the percent of energy transfer increases with the size of peptide. At higher energies an impulsive energy-transfer regime is reached where the size of the peptide has no effect on the energy-transfer efficiency. This study showed that as much as 80% of relative kinetic energy can be transferred upon collisions of polyglycines with Ar. Hase et al. also carried out classical trajectory simulations to study collisions of $Cr(CO)_6^+$ with self-assembled monolayers of *n*-hexyl thiolate.[22] The efficiency of T → V transfer slightly increased from 14 to 16% as the incident collision energy increased from 10 to 30 eV. The predicted amount of energy transfer is in good agreement with experimental findings. It should be noted that these estimates are referenced to the LAB kinetic energy for SID and to CM collision energy for CA.

We recently carried out energy-resolved studies of multiple-collision CID of $C_6H_5Br^{+\bullet}$ and $C_{10}H_7Br^{+\bullet}$ in FT-ICR.[23,24] Breakdown curves for individual fragmentation pathways were calculated using RRKM/QET formalism. Collision energy-resolved fragmentation efficiency curves obtained at different pressures were reconstructed based on the calculated breakdown graph and a proposed analytical form for the energy deposition function. The proposed collisional energy deposition function (CEDF) was shown to be flexible enough to reproduce experimental results obtained over a wide range of experimental parameters, e.g. collision energies and pressures. An exponential CEDF was deduced to fit the single-collision experiment, while the high-pressure collision limit for multiple-collision activation was described by a Boltzmann-like distribution of internal energies.[23] Thus the single-collision and high-pressure multiple collision limits correspond to both measured and expected physical limits for CA. We demonstrated that large amounts of internal energy could be deposited into the ion upon multiple-collision excitation, such that the energetics of fragmentation of both low- and high-energy channels can be investigated. Furthermore, the energetics of fragmentation of both a relatively simple ion ($C_6H_5Br^{+\bullet}$) and a much more complex system ($C_{10}H_7Br^{+\bullet}$) were successfully established using the described approach. This was achieved through RRKM-based modeling in which the amount of fragmentation observed is related to internal energy content rather than to the initial kinetic energy of the molecular ion, which is poorly defined in these classes of experiments.

In the past decade tandem mass spectrometry was successfully used to determine structures of various peptides and proteins. The peptide sequence can be reconstructed from the MS/MS mass spectrum based on the fragments that are formed from the molecular ion. The majority of fragments produced by low-energy CID and SID of protonated peptides correspond to charge-directed dissociation along the peptide backbone producing sequence-specific **b**, **a**, and **y** ions.[25−28] However, MS/MS spectra are frequently complicated by the presence of fragments corresponding to the loss of small neutral molecules from the protonated peptide or its subsequent fragments. Furthermore, some rearrangement products are also observed, especially on the long time scale characteristic of ion traps. The internal energy distribution of excited ions, the energetics and dynamics of fragmentation, and the instrumental time-window govern the

(16) Wysocki, V. H.; Kenttämaa, H. I.; Cooks, R. G. *Int. J. Mass Spectrom. Ion Processes* **1987**, *75*, 181.
(17) Vékey, K.; Brenton, A. G.; Beynon, J. H. *J. Phys. Chem.* **1986**, *90*, 3569.
(18) Vékey K.; Somogyi Á.; Wysocki, V. H. *J. Mass Spectrom.* **1995**, *30*, 212.
(19) Rakov, V. S.; Denisov, E. V.; Futrell, J. H.; Ridge, D. P. *Int. J. Mass Spectrom.* Submitted for publication.
(20) Marzluff, E. M.; Campbell, S.; Rodgers, M. T.; Beauchamp, J. L. *J. Am. Chem. Soc.* **1994**, *116*, 7787.
(21) Meroueh, O.; Hase, W. L. *J. Phys. Chem. A* **1999**, *103*, 3981.
(22) Bosio, S. B. M.; Hase, W. L. *Int. J. Mass Spectrom. Ion Processes* **1998**, *174*, 1.
(23) Laskin, J.; Byrd, M.; Futrell, J. H., *Int. J. Mass Spectrom.* **2000**, *195/196*, 285.
(24) Laskin, J.; Futrell, J. H. *J. Phys. Chem. A* **2000**, *104*, 5484.
(25) Biemann, K. *Methods Enzymol*. **1990**, *193*, 351, 455.
(26) Ballard, K. D.; Gaskell, S. J. *Int. J. Mass Spectrom. Ion Processes* **1991**, *111*, 173.
(27) Alexander, A. J.; Thibault, P.; Boyd, R. K. *Rapid Commun. Mass Spectrom.* **1989**, *3*, 30.
(28) McCormack, A. L.; Somogyi, Á.; Dongré, A. R.; Wysocki,V. H. *Anal. Chem.* **1993**, *65*, 2859.

type and amount of fragments observed in the mass spectrum. It follows that knowledge of peptide fragmentation energetics and mechanisms is essential for understanding and predicting the appearance of MS/MS mass spectra of peptides and proteins. Studying dissociation energetics of peptides and proteins is challenging because most of the well-developed experimental approaches that have been successfully employed in the studies of small and medium-size ions are simply not applicable to the fragmentation of large molecules, for which quantitative approaches are at an early stage of development.

Blackbody infrared dissociation (BIRD)[29−32] has been successfully used to study the energetics of fragmentation of large molecules. In this technique molecular ions are heated via blackbody infrared radiation inside the ICR cell. It has been shown that large ions can equilibrate with the blackbody radiation field and have internal energies given by a Boltzmann distribution. Arrhenius parameters for the dissociation of a variety of peptides and proteins have been reported.[31−35] Klassen and Kebarle studied the threshold energies for the formation of various fragment ions from protonated glycine, diglycine, triglycine, and their derivatives.[36] The procedure originally developed by Armentrout and co-workers[37,38] was used to extract activation energies from the observed fragmentation thresholds. Accurate activation energies could be obtained for the fragmentation of glycine, glycinamide, and the formation of immonium ion ($\mathbf{a_1}$) from (Gly-Gly)H^+. However, dissociation thresholds for larger precursor ions were affected by substantial kinetic shifts and accurate activation energies for these reactions could not be obtained. Vachet and Glish determined relative dissociation energies of a series of small protonated peptides using a boundary-activated dissociation (BAD) technique in a quadrupole ion trap.[39]

Wysocki and co-workers estimated average activation energies of a series of protonated peptides based on the collision energy-resolved SID data.[40] They found that the activation energies of nonbasic peptides were smaller than the activation energies of basic peptides of similar size. These results are in agreement with the mobile proton model of peptide fragmentation.[26−28,41,42] However, the absolute value of the activation energy of leucine enkephalin obtained in this study (1.56 eV)[40] was significantly higher than the value obtained using BIRD (1.09 eV).[35] Hanley and co-workers developed a method for determination of relative dissociation energies from SID thresholds.[43,44] Relative dissociation energies (RDEs) for the major fragment ions of triglycine, tetraglycine, leucine enkephalin, and leucine enkephalin arginine were obtained using this method.[45] The proposed modeling requires knowledge of the kinetic-to-internal energy conversion (T → V) and the energy dissipated into the surface that are usually ill defined. Cancilla et al. studied collision energy-resolved dissociation of a series of oligosaccharides under multiple collision conditions using FT-ICR.[46] Multicollision dissociation threshold (MCDT) values, which provide relative reaction thresholds for different fragmentation channels, were determined from the kinetic energy dependence of the CID products. Unfortunately, application of FT-ICR for threshold measurements is severely constrained by the limited dynamic range of this instrument. Thus the above approach will require very high signal intensities to obtain accurate threshold values using FTMS.

The present work is a continuation of our group's effort to develop a methodology that will allow exploring fragmentation of large molecules using multiple-collision activation (MCA-CID) and SID techniques. Our study on the energetics of fragmentation of bromobenzene and bromonaphthalene radical cations revealed that modeling of the collision energy-resolved fragmentation efficiency curves over a wide range of collision energies had the singular advantage that it was insensitive to experimental uncertainties.[23,24] We anticipate using the same approach to understand the mechanistic details of peptide fragmentation. We present here a detailed investigation of the fragmentation of protonated dialanine (Ala-AlaH^+) using MCA-CID and SID in a Fourier Transform Ion Cyclotron Resonance Mass Spectrometer (FT-ICR MS). For the first time a direct comparison between the energy-resolved fragmentation efficiency curves obtained using both methods was possible. This study is unique in the sense that both methods were implemented on the same instrument enabling a quantitative comparison of the experimental results.

Experimental Section

Experiments were performed on the University of Delaware 7T Bruker BioApex FT-ICR mass spectrometer equipped with a commercial electrospray source (Analytica of Branford, Branford, CT). The system is operated at an indicated base pressure of 5×10^{-10} Torr. Dialanine was purchased from Sigma (St. Louis, MO) and used without further purification. The sample was dissolved in 50:50 (v/v) water−methanol solution containing a small amount of acetic acid (<1%). Sample solutions were infused into the ESI source using a Harvard Apparatus (Natick, MA) syringe pump at a flow rate of 10−50 μL/h.

SID Experiments. Detailed description of the experimental setup for SID experiments was given elsewhere.[47] Briefly, the surface was introduced into the ICR cell through the aperture in the rear ICR trapping plate at 90° to the magnetic field. The surface holder was in electrical contact with the back trapping plate. Ions produced in the ESI source were accumulated in the hexapole and extracted after a delay of 0.4 s by a 100 μs extraction pulse. The ions were transferred into the ICR cell by a series of lenses. The ion's kinetic energy was varied by floating the hexapole rods, skimmer, and hexapole extraction plate using an external power supply. The SID collision energy was determined as a difference between the source offset and the target potentials. Slightly asymmetric potential was created in the ICR cell by applying 5 V to the front trapping plate and 2 V to the rear plate and the surface. It has been shown previously that the kinetic energy

(29) Dunbar, R. C. *J. Phys. Chem.* **1994**, *98*, 8705.
(30) Price, W. D.; Schnier, P. D.; Williams, E. R. *Anal. Chem.* **1996**, *68*, 859.
(31) Price, W. D.; Schnier, P. D.; Jockusch, R. A.; Strittmatter, E. F.; Williams, E. R. *J. Am. Chem. Soc.* **1996**, *118*, 10640.
(32) Dunbar, R. C.; McMahon, T. B. *Science* **1998**, *279*, 194 and references therein.
(33) Price, W. D.; Schnier, P. D.; Williams, E. R. *J. Phys. Chem. B* **1997**, *101*, 664.
(34) Schnier, P. D.; Price, W. D.; Jockusch, R. A.; Williams, E. R. *J. Am. Chem. Soc.* **1996**, *118*, 7178.
(35) Schnier, P. D.; Price, W. D.; Strittmatter, E. F.; Williams, E. R. *J. Am. Soc. Mass Spectrom.* **1997**, *8*, 771.
(36) Klassen, J. S.; Kebarle, P. *J. Am. Chem. Soc.* **1997**, *119*, 6552.
(37) Rodgers, M. T.; Ervin, K. M.; Armentrout, P. B. *J. Chem. Phys.* **1997**, *106*, 4499.
(38) Rodgers, M. T.; Armentrout, P. B. *J. Chem. Phys.* **1998**, *109*, 1787.
(39) Vachet, R. W.; Glish, G. L. *J. Am. Soc. Mass Spectrom.* **1998**, *9*, 175.
(40) Vékey, K.; Somogyi, Á.; Wysocki,V. H. *Rapid Commun. Mass Spectrom.* **1996**, *10*, 911.
(41) Dongré, A. R.; Jones, J. L.; Somogyi, Á.; Wysocki,V. H. *J. Am. Chem. Soc.* **1996**, *118*, 8365.
(42) Nair, H.; Wysocki,V. H. *Int. J. Mass Spectrom. Ion Processes* **1998**, *174*, 95.
(43) Wainhaus, S. B.; Gislason, E. A.; Hanley, L. *J. Am. Chem. Soc.* **1997**, *119*, 4001.
(44) Lim, H.; Schultz, D. G.; Gislason, E. A.; Hanley, L. *J. Phys. Chem. B* **1998**, *102*, 4573.
(45) Lim, H.; Schultz, D. G.; Yu, C.; Hanley, L. *Anal. Chem.* **1999**, *71*, 2307.
(46) Cancilla, M. T.; Wong, A. W.; Voss, L. R.; Lebrilla, C. B. *Anal. Chem.* **1999**, *71*, 3206.
(47) Rakov, V. S.; Futrell, J. H.; Denisov, E. V.; Ridge, D. P. *Eur. Mass Spectrom.* In press.

of the ions after collision with the surface is about 1 eV under the experimental conditions described here.[47] Secondary ions produced by surface impact are slightly accelerated toward the center of the cell and turned around by the 5 V potential applied to the front trapping plate. At this time the dynamic voltage trapping (DVT) is activated by applying a 7 V potential to both trapping plates. Delay time between the hexapole extraction and the activation of the DVT was chosen based on SIMION simulation of the ion's trajectories. The delay varied from 200 to 65 μs when the collision energy changed from 5 to 23 eV. After an additional delay of 1 s the ions were excited for detection by broadband chirp excitation (SID mass spectra acquired using a longer delay time of 5 s were identical with the spectra obtained using 1 s delay).

SAMs were prepared on a solid gold disk soldered onto the surface holder. Prior to depositing the self-assembled monolayers onto the gold surface, the holder was irradiated using a Boekel Industries Inc. (model 135500) UV cleaner for 10 min. The whole copper−gold assembly was then immersed for at least 24 h in a 1 mM ethanol solution of the FC_{12} alkanethiol ($CF_3(CF_2)_9C_2H_4SH$). Extra layers of the SAMs were removed by four-stage rinsing (10 min ultrasonic cleaning) of the assembly in ethanol.

SORI-CID Experiments. We recently described the experimental conditions for well-defined collision energy-resolved SORI-CID measurements.[23] Ions generated in an electrospray source are accumulated in a hexapole for a predefined trapping time that was approximately 1 s in these experiments. The ions are extracted from the hexapole, transferred into the ICR cell by a series of ion transfer lenses, and captured in the cell using the Sidekick mechanism for ion accumulation. Ions were trapped in the cell by applying a 2 V potential to the trapping plates. Excess kinetic energy was removed from the ions by pulsing Ar into the cell for a duration of about 300 ms at a maximum pressure of 2×10^{-6} Torr. Ions were allowed to cool to thermal equilibrium by radiative and collisional cooling during the pumping delay of 5 s. The precursor ion was isolated using a correlated sweep procedure. A second Ar pulse was then introduced to remove any excess kinetic energy gained by the molecular ions during the isolation event. A third Ar pulse was introduced into the cell for collisional activation. We have measured the time-dependent pressure of Ar in the cell previously.[23] The pressure profile shows a peak in pressure at ca. 100−120 ms delay time between the pulse valve opening and detection event and fwhm of about 170 ms. Ion activation was performed during the time when the pressure was close to its maximum. Protonated molecular ions were radially excited slightly off-resonance ($\Delta f = -700$ Hz) for 100 ms at nearly fixed Ar pressure. Pressure calibration described by us previously[23] was used throughout this work. The kinetic energy of the ions was incremented by changing the peak-to-peak voltage applied to the excitation plates. After a 5 s pumping delay the ions were excited for detection by broadband chirp excitation.

From the set of spectra obtained at different collision energies, a plot of the relative precursor and fragment ion abundance as a function of the center-of-mass energy of the precursor ion for CID experiments and laboratory energy for SID experiments was constructed. We refer to these curves as fragmentation efficiency curves (FECs). CID experiments presented in this study were conducted at two pressures corresponding to collision numbers of 5 and 15 (collision cross section of 95 Å^2 for Ala-AlaH$^+$ collisions with Ar was estimated based on the ion mobility data[48]). We have demonstrated[23,24] that fragmentation efficiency upon multiple-collision activation is substantially enhanced when collision number increases from 3 to 15. However, at higher pressures no further enhancement of the fragmentation efficiency was observed. This "saturation" effect is probably a result of essential thermalization of the system at a collision number of 15 and above. In this case further increase in pressure will not affect the fragmentation efficiency but will result in a more pronounced ion loss.

Double resonance experiments combined with SORI excitation were performed by applying an additional radio frequency wave simultaneously with the SORI excitation pulse with a frequency corresponding to the cyclotron frequency of the ion to be ejected and an amplitude of 50 V. Duration of the ejecting pulse (typically 3 s) was chosen to be long enough to allow ejection of the ions formed both during the SORI excitation pulse and after the excitation wave has been switched off. Basic considerations for a choice of RF amplitude of the ejection wave and possible reasons for incomplete ejection were discussed elsewhere.[24]

(48) Hudgins, R. R.; Mao, Y.; Ratner, M. A.; Jarrold, M. F. *Biophys. J.* **1999**, *76*, 1591.

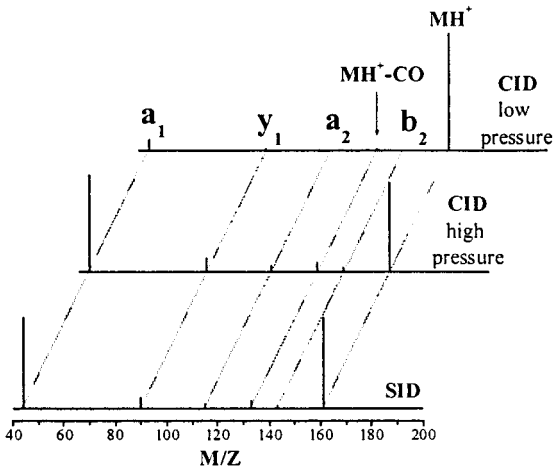

Figure 1. Representative MCA-CID mass spectra corresponding to the CM energy of 3 eV (top panel) and SID spectrum at 11.5 eV incident collision energy (bottom panel).

Results and Discussion

MCA-CID and SID Fragmentation Efficiency Curves. Energy-resolved MCA-CID mass spectra were collected at two different pressures, corresponding to collision numbers of 5 and 15 and maximum center-of-mass energies from 0 to 5 eV. SID mass spectra were obtained for collision energies between 3 and 23 eV. Representative MCA-CID mass spectra corresponding to the CM energy of 3 eV and SID spectrum at 11.5 eV incident collision energy are shown in Figure 1. Fragmentation of protonated dialanine leads mainly to a formation of immonium ion (a_1). Other ions observed in the mass spectra are b_2 (m/z 143), a_2 (m/z 115), y_1 (m/z 90), and m/z 133 corresponding to the loss of CO from the parent ion.[49] The same fragments were observed in both CID and SID experiments. Fragmentation efficiency of MCA-CID increases dramatically with a 3-fold rise in Ar pressure. It is interesting to note that the high-pressure CID and SID mass spectra shown in Figure 1 are very similar.

SID and MCA-CID fragmentation efficiency curves are compared in Figures 2a−f. MCA-CID curves are plotted as a function of maximum center-of-mass (CM) collision energy, while the energy scale of SID curves (E_{SID}) was converted to an "effective" CM energy (E_{CM}^{SID}) with an arbitrary neutral encounter of mass M_N using the following relationship:

$$E_{CM}^{SID} = \frac{M_N}{M_N + M_{ion}} E_{SID} \qquad (1)$$

The best overlap between the SID and MCA-CID fragmentation efficiency curves (FECs) shown in Figure 2 was obtained for $M_N = 46$. It is interesting to note that an average value of 43 ± 3 for M_N was obtained by us from the comparison of MCA-CID and SID of a series of alanine-containing peptides (manuscript in preparation). It would be interesting to explore the dependence of M_N on different parameters, such as peptide

(49) In the case of dialanine the loss of 28 mass units can be due to the loss of either CO or C_2H_4 from the parent ion. We performed the accurate mass measurement that confirmed that a fragment at m/z 133 corresponds to the loss of CO rather than C_2H_4.

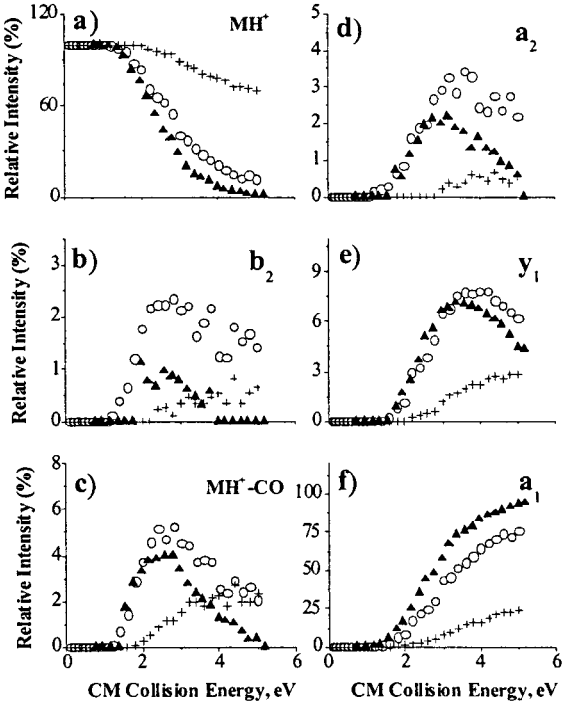

Figure 2. Comparison of the fragmentation efficiency curves obtained in SID (▲) and low- (+) and high-pressure (○) MCA-CID experiments for (a) MH^+, (b) b_2, (c) MH^+-CO, (d) a_2, (e) y_1, and (f) a_1 ions.

mass, size and sequence, surface characteristics, collision energy, etc. However, these questions are beyond the scope of the present work.

Surprisingly, the SID and MCA-CID curves are very alike. Since the time scales of the SID and CID experiments reported here are very close to each other, both experiments can be described by the same breakdown graph (fragmentation probability). Since FEC is a product of the energy-dependent fragmentation probability and the energy deposition function, the similarity between SID and CID results indicates that the internal energy distributions of dialanine activated by multiple collisions and by surface impact are very similar. This finding disagrees with the generally accepted assertion that SID produces much narrower internal energy distributions than CID. However, to the best of our knowledge, no direct comparison between the two activation techniques, utilizing the same apparatus, has been reported thus far. It will be instructive to compare these two techniques using peptides of different size and sequence prior to drawing general conclusions on the similarities and differences between MCA-CID and SID. These questions will be addressed in a forthcoming publication.

For protonated dialanine we conclude that the excitation mechanism upon ion−surface impact is very similar to the high-pressure multiple-collision activation. Since we have shown previously that high-pressure multiple collision activation produces an ensemble of ions with an internal energy distribution close to a thermal distribution,[23] we may also conclude that ions activated by surface impact approach a thermal distribution of internal energies. The simplest rationalization of these observations is that ions undergo multiple interactions with the surface prior to expulsion. This may involve penetration of projectile ions into the self-assembled monolayer and almost certainly involves interaction of many of the constituent atoms of the complex ion with the surface.

Dissociation Pathways. Double-resonance experiments were performed to verify dissociation pathways of dialanine and its fragments. In these experiments a selected fragment is continuously ejected from the ICR cell during the SORI excitation. The ejecting radio frequency wave is continued for 3 additional seconds after the SORI excitation pulse is turned off to ensure a complete ejection of all the ions of the selected mass-to-charge ratio. As a result of ejection of a particular fragment ion, intensities of all the ions for which it is a precursor are strongly reduced. These experiments were performed with a SORI excitation voltage that corresponds to the maximum center-of-mass collision energy of 5 eV and Ar pressure corresponding to a collision number of 15. Under these CID conditions all fragment ions of interest are present in a normal SORI-CID spectrum. The intensity of the a_2 ion (*m*/*z* 115) drops to less than 10% of its original intensity upon ejection of the b_2 ion (*m*/*z* 143), indicating that a_2 ions are mainly formed by sequential fragmentation of b_2 ions.[50] This agrees with results obtained by Harrison and co-workers[60] from kinetic energy release measurements for the fragmentation of protonated dipeptides. Since the intensities of b_2, y_1, P-CO, and a_1 ions were not affected by ejection of any other ions from the system, we concluded that these fragments are formed directly from the parent ion. However, the high-pressure SORI-CID fragmentation efficiency curves for a_2, y_1, and P-CO are strongly depleted at high collision energies because of sequential fragmentation of these species. The only product that can be formed from a_2 and y_1 is the immonium ion (a_1, *m*/*z* 44). P-CO can dissociate via a loss of water to yield the a_2 ion. However, the intensity of *m*/*z* 115 (a_2) was not affected by ejection of the P-CO ion. This suggests that in our experiments a_2 ions are not formed from P-CO. We infer that the most probable fragmentation pathway for P-CO leads to formation of the a_1 ion. Thus although most a_1 ions are formed directly from the parent ion, there is some contribution from secondary fragmentation to the intensity of the immonium ion. The observed fragmentation pathways are summarized in Scheme 1.

Scheme 1

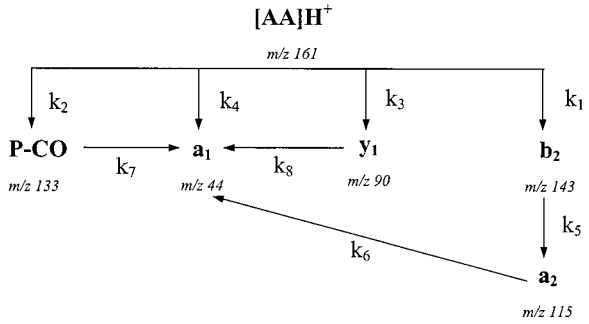

(50) The remaining 10% of a_2 ions could be formed directly from the parent ion. However, most likely these ions are observed due to the unimolecular or CID decay of b_2 ions during ejection.

(51) Lifshitz, C. *Adv. Mass Spectrom.* **1989**, *11*, 113.
(52) Vestal, M. L. *J. Chem. Phys.* **1965**, *43*, 1356.
(53) Bente, P. F., III; McLafferty, F. W.; McAdoo, D. J.; Lifshitz, C. *J. Phys. Chem.* **1975**, *79*, 713.
(54) Cordero, M. M.; Houser, J. J.; Wesdemiotis, C. *Anal. Chem.* **1993**, *65*, 1594.
(55) Reid, G. A.; Simpson, R. J.; O'Hair, R. A. J. *Int. J. Mass Spectrom.* **1999**, *190/191*, 209.
(56) Schnier, P. D.; Jurchen, J. C.; Williams, E. R. *J. Phys. Chem. B* **1999**, *103*, 737.
(57) Nold, M. J.; Wesdemiotis, C.; Yalcin, T.; Harrison, A. G. *Int. J. Mass Spectrom. Ion Processes* **1997**, *164*, 137.
(58) Yalcin, T.; Khouw, C.; Csizmadia, I. G.; Peterson, M. R.; Harrison, A. G. *J. Am. Soc. Mass Spectrom.* **1995**, *6*, 1165.
(59) Yalcin, T.; Csizmadia, I. G.; Peterson, M. R.; Harrison, A. G. *J. Am. Soc. Mass Spectrom.* **1996**, *7*, 233.

Theoretical Modeling. Modeling of energy-resolved fragmentation efficiency curves was described by us previously.[23,24] Briefly, energy-dependent microcanonical rate constants for all reaction channels were calculated using RRKM/QET. Fragmentation probability as a function of the internal energy of the parent ion and the experimental observation time (t_r), $F(E,t_r)$, was calculated from the rate-energy k(E) dependencies. The energy deposition function was described by the following analytical expression:

$$P(E,E_{coll}) = (E - \Delta)^l \exp[-(E - \Delta)/f(E_{coll})]/C \qquad (2)$$

where l and Δ are parameters, $C = \Gamma(l + 1)[f(E_{coll})]^{l+1}$ is a normalization factor, and $f(E_{coll})$ has the form:

$$f(E_{coll}) = A_2 E_{CM}^{\ 2} + A_1 E_{CM} + A_0 \qquad (3)$$

where A_0, A_1, and A_2 are parameters. For MCA-CID results A_0 was replaced with $E_{th}/(l + 1)$, where E_{th} is the average thermal energy of protonated dialanine at 298 K.[23,24] E_{coll} equals the collision energy for SID experiments and the maximum center-of-mass collision energy for MCA-CID experiments.

Since the contribution of ions having internal energy, E, to the observed signal intensity for a particular reaction channel, i, equals $F_i(E,t_r)\ P(E,E_{CM})$, the normalized signal intensity for a particular reaction channel is given by the equation:

$$I_i(E_{coll}) = \int_0^\infty F_i(E,t)\ P(E,E_{coll})\ dE \qquad (4)$$

Calculated fragmentation efficiency curves were constructed from the energy-dependent signal intensities for the precursor ion and its fragments. The results were compared to the experimental FECs and the fitting parameters varied until the best fit to experimental fragmentation efficiency curves was obtained. The fitting parameters included critical energies of all reactions (Scheme 1), activation entropies of reactions 1−4, parameters characterizing the energy deposition function (eqns 2 and 3), and the rate of radiative decay of the protonated dialanine. We found that calculated FECs were insensitive to the activation entropies of reactions 5−8.

In the present study we used the same approach to model the fragmentation efficiency curves obtained in MCA-CID and SID experiments. The reaction time of 5 s was used to calculate the breakdown graph appropriate for MCA-CID experiments and 1 s was used for SID experiments. Calculated breakdown graphs for 1 and 5 s were identical, indicating that $t = 1$ s can be considered as infinite time for the reaction system presented by Scheme 1.

RRKM Parameters. AM1 calculations were used to estimate vibrational frequencies of protonated dialanine and its fragments. It is well accepted that RRKM calculations are not sensitive to the details of vibrational frequencies of the molecular ion and transition states but rather to the relative change in frequencies along the reaction coordinate characterized by activation entropy ($\Delta S^{\ddagger}$).[51] Thus we feel that a more elaborate modeling of vibrational frequencies is unnecessary in the context of the present investigation. Vibrational frequencies of transition states were estimated in the following way: one frequency in the range of 1000−1500 cm^{-1}, corresponding to C−N, C−O, or C−C stretch (depending on the reaction), was chosen as a reaction coordinate and other 8 frequencies in the range 300−1500 cm^{-1} were varied to obtain the best fit with experimental data.

(60) Ambihapathy, K.; Yalcin, T.; Leung, H.-W.; Harrison, A. G. *J. Mass Spectrom.* **1997**, *32*, 1997.

Energy Partitioning. The internal energy of an ionic fragment formed from a precursor ion with internal energy E will be equal to $E - E_0$ (where E_0 is the critical energy for the reaction) only in the case when a neutral fragment does not contain any internal energy. This happens only when the neutral fragment does not have any vibrational degrees of freedom. However, the above relationship will fail if the neutral fragment is polyatomic. In this case the internal energy of the ionic fragment is less than $E - E_0$ and the fraction of the internal energy carried off by the neutral increases with increasing complexity of the neutral fragment. In our study of the fragmentation of bromonaphthalene radical cation we have shown that partitioning of energy between the ionic and neutral products must be included in the modeling of the fragmentation kinetics of complex systems.[24] This can be done (assuming that the excess energy is partitioned statistically among the fragments) by calculating all permutations of the energy partitioning from densities of states of the ionic and neutral fragments. Given the total internal energy in the precursor ion (E), the probability that an energy between ϵ and $\epsilon + d\epsilon$ remains internal energy of ionic fragment is given by: [52,53]

$$p(E,\epsilon) = \frac{\rho_1(\epsilon)\rho_2(E - E_0 - \epsilon)\ d\epsilon}{\int_0^{E-E_0} \rho_1(\epsilon)\rho_2(E - E_0 - \epsilon)\ d\epsilon} \qquad (5)$$

where ρ_1 and ρ_2 are the densities of states of ionic and neutral fragments, respectively, and E_0 is the critical energy for reaction.

The internal energy content of $\mathbf{b_2}$, **P-CO**, $\mathbf{a_2}$, and $\mathbf{y}_1$ ions was estimated based on the probability distributions given by eq 5. This information was used to calculate the rates of subsequent fragmentation of these ions. The most probable internal energy (E_{mp}) as a function of $E - E_0$ was extracted from the calculated probability distributions. These calculations revealed that the internal energy content of $\mathbf{b_2}$, **P-CO**, and $\mathbf{a_2}$ could be well approximated by $E - E_0$ because their formation is accompanied by formation of relatively small neutral fragments (H_2O and CO). However, the internal energy of the $\mathbf{y_1}$ ion is substantially lower than $E - E_0$ because the neutral fragment (C_3H_5NO) formed by reaction 3 can carry off a significant amount of internal energy. Neutralization−reionization experiments have shown that C_3H_5NO that accompanies formation of the $\mathbf{y_1}$ ion has the structure of a cyclic aziridinone as shown in Scheme 2.[54] Vibrational frequencies of C_3H_5NO were estimated using

Scheme 2

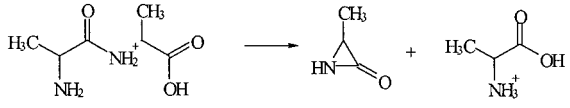

AM1 calculations. The most probable internal energy extracted from the probability distributions was plotted as a function of $E - E_0$. The dependence of E_{mp} on $E - E_0$ was approximated by the second-order polynomial, and the analytical expression for E_{mp} obtained in this way was used to calculate the rate-energy dependence of the unimolecular rate constant for reaction 8. A small correction was introduced to the internal energies of $\mathbf{b_2}$, **P-CO**, and $\mathbf{a_2}$ using the same procedure. These results are summarized in Figure 3. The line corresponding to $E_{mp} = E - E_0$ is shown for comparison.

Results of RRKM Modeling

1. Rate Constants, Breakdown Graph, and Fragmentation Efficiency Curves. The results of theoretical modeling are

Table 1. RRKM/QET Parameters

experiment	reaction	**1** P→ b_2	**2** P → (P−CO)	**3** P → y_1	**4** P → a_1	**5** b_2 → a_2	**6** a_2 → a_1	**7** (P−CO) → a_1	**8** y_1 → a_1
MCA-CID	E_0, eV	1.92	1.84	1.98	2.00	0.95	1.01	0.94	1.5−2.2
$n = 5$	$\Delta S^{\ddagger}$, eu[a]	0.94	0.06	5.36	10.36	−	−	−	−
MCA-CID	E_0, eV	1.95	1.96	2.08	2.18	1.00	0.95	0.89	1.66
$n = 15$	$\Delta S^{\ddagger}$, e.u.[a]	−1.70	1.93	3.88	10.36	−	−	−	−
SID	E_0, eV	1.95	1.96	2.13	2.16	0.98	0.94	0.92	1.68
	$\Delta S^{\ddagger}$, eu[a]	−4.5	1.1	3.8	9.1	−	−	−	−
Average	E_0, eV	1.94 (0.10)	1.92 (0.12)	2.06 (0.11)	2.11 (0.15)	0.98 (0.07)	0.97 (0.07)	0.92 (0.06)	1.67 (0.35)
	$\Delta S^{\ddagger}$, eu[a]	−1.8 (2.1)	1.0 (1.0)	4.3 (1.0)	9.9 (1.0)	−	−	−	−

[a] Activation entropies for reactions 5−8 could not be determined because the results of theoretical modeling were not sensitive to these parameters. [b] Uncertainties shown in parentheses were determined from the sensitivity analysis.

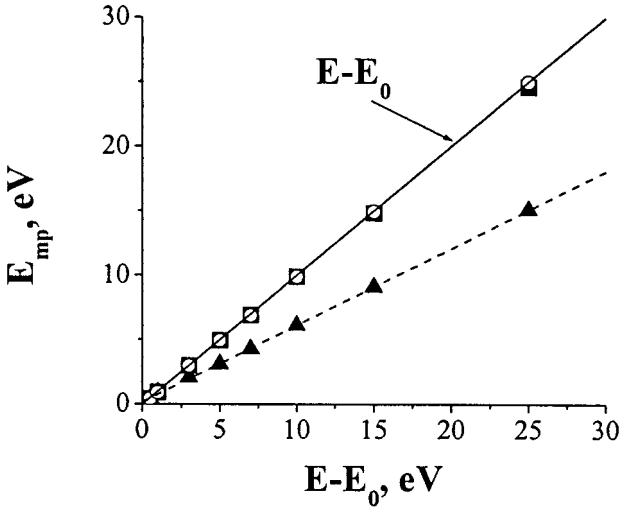

Figure 3. The most probable internal energy deposited into (○) the a_2 ion, (■) b_2, and (▲) the y_1 ion as a function of $E - E_0$. The line corresponding to $E_{mp} = E - E_0$ is shown for comparison. The dashed line represents the polynomial fit for E_{mp} of the y_1 ion.

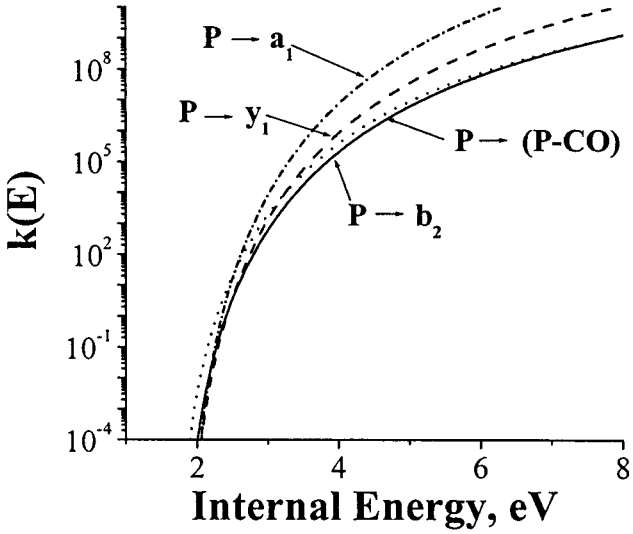

Figure 4. RRKM rate−energy dependencies for the four primary fragmentation pathways of Ala-AlaH$^+$: (—) reaction 1; (···) reaction 2; (- - -) reaction 3; and (— · —) reaction 4.

summarized in Table 1. Sensitivity analysis was performed for all three experiments (low- and high-pressure CID and SID) by systematically changing the critical energy of reaction 1 in increments of 0.02 eV and adjusting the rest of the fitting parameters to give the best fit. The error bars for each experiment (not shown in the table) were obtained in this way. The radiative decay rate which gave the best agreement with the experimental FECs is 40 ± 15 s^{-1}. Microcanonical rate constants for reactions 1−4 are shown in Figure 4. Rate-energy dependencies for reactions 5−8 are not presented because modeling was not sensitive to the activation entropies of these reactions. Basically, reactions 5−8 could be treated in the "sudden death" approximation, meaning that even at very low excess internal energy the reaction rate is much faster than the rate constant sampled experimentally and the reaction takes place immediately provided the internal energy is above the dissociation threshold.

The lack of sensitivity of the modeling to some of the parameters can be rationalized based on the following considerations: Rate constants sampled in our experiments are very small because of the relatively long reaction times (5 s for MCA-CID and 0.2 s for SID). Small rate constants correspond to a relatively low internal excitation, at which the rate-energy dependencies of microcanonical rate constants are determined primarily by the critical energy for dissociation. At higher excitation, sampled by a shorter time-window of a conventional mass spectrometer, the activation entropy is an important parameter. Therefore the results obtained on any mass spectrometer characterized by a short time scale will depend on both the critical energies and activation entropies. In contrast, the results obtained on a long time scale depend only on the critical energies. However, for competing reactions both the critical energies and the activation entropies of the reactions determine the branching ratio between the products even at very low internal excitations. Therefore, the results of the present modeling of the competing reactions 1−4 are sensitive to both energetics and dynamics.

Breakdown curves for the fragmentation of protonated dialanine presented in Figure 5 were calculated from the rate-energy dependencies for reaction time of 5 s sampled in our MCA-CID experiments. Very similar breakdown curves corresponding to a reaction time of 0.2 s were obtained for SID experiments (not shown). The stepwise formation of the immonium ion (**a_1**) above 3 eV is due to a consecutive fragmentation of **a_2** and **y_1** ions. It is clear that the immonium ion (**a_1**) should be observed as a dominant fragment over a wide range of energies. Although the critical energy for the formation of the **b_2** ion is relatively low this fragment is produced in small amount because of the low activation entropy associated with its formation. Both (**P-CO**) and **b_2** ions are relatively unstable and readily fragment to yield **a_1** and **a_2** ions, respectively. The breakdown curve for the **y_1** ion is broad because (a) this

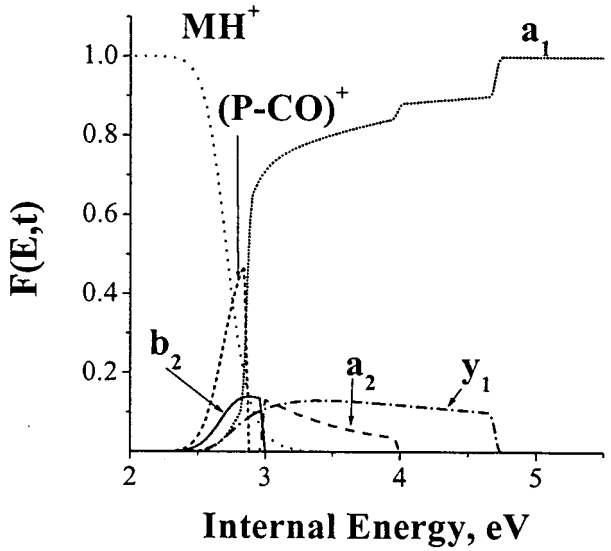

Figure 5. Calculated breakdown curves for the fragmentation of Ala-AlaH$^+$ and the reaction time of 5 s.

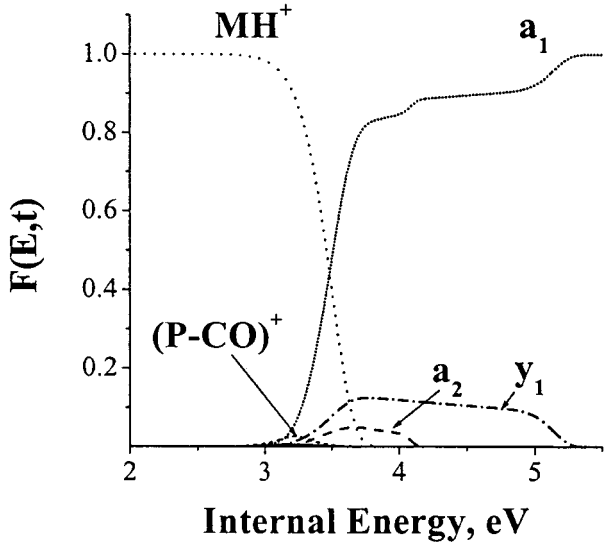

Figure 6. Calculated breakdown curves for the fragmentation of Ala-AlaH$^+$ and the reaction time of 20 μs.

fragment is relatively stable (it requires ca. 1.7 eV to dissociate) and (b) formation of $\mathbf{y_1}$ by reaction 4 is accompanied by formation of a large neutral fragment that can carry off a substantial amount of internal energy as discussed earlier. Thus additional excitation is required to induce fragmentation of the $\mathbf{y_1}$ ion. The interplay between these two factors leads to a broad breakdown curve and, consequently, a relatively large amount of the $\mathbf{y_1}$ ion present in the mass spectrum.

Klassen and Kebarle studied the CID of protonated diglycine (Gly-GlyH$^+$) in a triple quadrupole mass spectrometer.[36] They found that single-collision activation of Gly-GlyH$^+$ results exclusively in the formation of $\mathbf{y_1}$ and $\mathbf{a_1}$ ions. The reaction time of 23 μs was sampled in these experiments. However, Reid et al. observed losses of water and CO from protonated diglycine following collisional activation in a quadrupole ion trap.[55] To gain a better understanding on the influence of the reaction time on the appearance of CID mass spectra we calculated the breakdown graph for Ala-AlaH$^+$ for the short reaction time. The results are presented in Figure 6. It is clear that on a short time scale of the triple quadrupole mass spectrometer the intensities of both $\mathbf{b_2}$ and **(P-CO)** ions are strongly depleted.

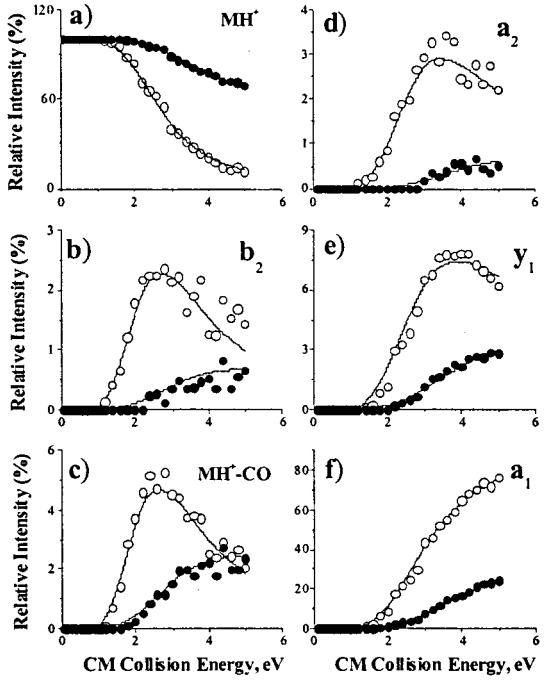

Figure 7. Collision energy-resolved SORI-CID fragmentation efficiency curves and the results of theoretical modeling (solid lines): (●) low-pressure experiment (collision number $n = 5$) and (○) high-pressure experiment (collision number $n = 15$); (a) MH$^+$, (b) b_2, (c) MH$^+$−CO, (d) a_2, (e) y_1, and (f) a_1.

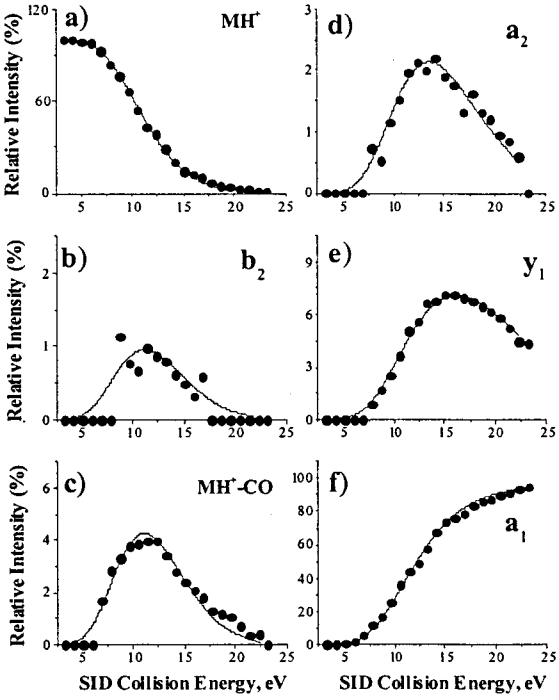

Figure 8. Collision energy-resolved SID fragmentation efficiency curves and the results of theoretical modeling for (a) MH$^+$, (b) b_2, (c) MH$^+$−CO, (d) a_2, (e) y_1, and (f) a_1 ions.

Thus these ions cannot be detected on a microsecond time scale. Furthermore, a substantial kinetic shift of 0.78 eV (18 kcal/mol) is obtained from the comparison of the breakdown curves calculated for 20 μs and 5 s. This value is in close agreement with the value of 20 kcal/mol found by Klassen and Kebarle[36] for protonated diglycine.

Figures 7 and 8 show the comparison between the experimental and calculated fragmentation efficiency curves for MCA-

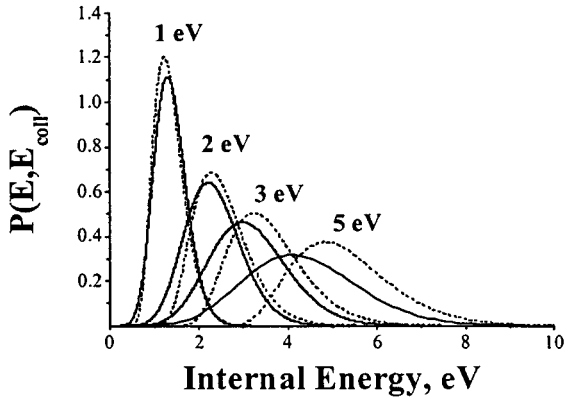

Figure 9. Internal energy distributions upon multiple-collision (solid lines) and ion−surface impact (dashed lines). MCA-CID distributions corresponding to the maximum center-of-mass (CM) energy of 1, 2, 3, and 5 eV. The SID collision energy was converted to an "effective" CM energy assuming the mass of neutral encounter on the surface of 46 amu.

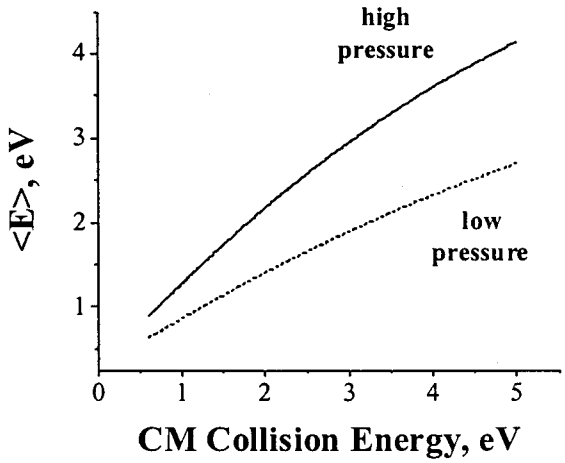

Figure 10. Average internal energy transferred upon collisions with Ar as a function of the maximum center-of-mass energy of the parent ion for the low-pressure (dashed line) and the high-pressure (solid line) experiments.

CID and SID experiments, respectively. The agreement between the experiment and the model is fairly good. It is remarkable that both CID and SID experiments could be fitted within the same model confirming that these two activation techniques are very similar in nature.

2. Energy Deposition Function. The proposed analytical form for the energy deposition function given by eqs 2 and 3 can be used to model the energy transfer in both MCA-CID and SID experiments. We have shown previously that this function transforms to a simple exponential EDF for a single-collision experiment and a Boltzmann-like bell-shaped EDF for multiple-collision experiments.[23] The comparison between the internal energy distributions that gave the best fit to the SID and high-pressure (collision number 15) CID experiments is presented in Figure 9. Internal energy distributions for multiple-collision activation shown in Figure 9 correspond to maximum center-of-mass collision energies of 2, 3, and 5 eV, while the SID collision energy was scaled to an "effective" CM energy using eq 1 and a neutral mass (M_N) of 46 amu. As pointed out earlier (see section MCA-CID and SID Fragmentation Efficiency Curves), the best overlap of MCA-CID and SID fragmentation efficiency curves was obtained with this value of M_N. The SID distributions are slightly more asymmetric than the corresponding CID distributions. Interestingly, the internal energy distributions obtained upon SID are only slightly narrower than the distributions for multiple-collision activation. This result is in disagreement with the generally accepted opinion that "SID offers deposition of a narrow distribution of internal energy".[12,13] However, this conclusion was drawn out from the comparison of high-energy single-collision activation with SID and no detailed comparison of multiple-collision activation and SID has been performed so far. We have recently compared internal energy distributions of ions activated by single and multiple collisions.[23] The results clearly indicated that the single-collision EDF is substantially narrower than the EDF corresponding to multiple-collision activation provided the center-of-mass collision energy is the same. The distribution broadens, as expected, with increase in the CM collision energy. It is important to note that only the high-pressure MCA-CID results are comparable to the SID fragmentation efficiency curves. Thus care should be taken in choosing the experimental conditions for multiple-collision activation to obtain accurate comparison between these two techniques.

Another interesting observation is that while the SID and CID internal energy distributions overlap reasonably well at low collision energies they diverge significantly at higher energies. The differences between the distributions may result from several factors:

(1) At high collision energies the fragments produced by multiple-collision activation can be deactivated by collisions with neutral gas that is still present in the ICR cell. Since in the present study the internal energy content of the ion is derived from its fragmentation efficiency, collisional deactivation will result in the observation of the lower average energy deposited upon collisions and somewhat narrower internal energy distribution.

(2) The mass of neutral encounter for the surface impact (M_N) used to convert the SID collision energy from the laboratory frame to the "effective" CM frame can vary with collision energy. Thus it is hard to conclude on the basis of the present results whether the use of 46 amu for the mass of neutral encounter on the surface is applicable to the whole energy range sampled experimentally.

The average internal energy deposited into the precursor ion upon multiple-collision activation is shown in Figure 10 as a function of the maximum CM collision energy. Obviously, the enhanced energy transfer is observed in the high-pressure experiment ($n = 15$) as compared to the low-pressure ($n = 5$) results. The average energy was converted into the "effective" temperature of the precursor ion using the known vibrational frequencies of the precursor ion and the standard relationship between average energy and temperature from statistical thermodynamics. The results are summarized in Table 2. The 3-fold rise in pressure results in about a 60% increase in the average internal energy and about a 35% increase in the "effective" temperature.

We have recently shown that the "effective" temperatures of $C_6H_5Br^{+\bullet}$ and $C_{10}H_7Br^{+\bullet}$ were the same for both ions for the same bath gas pressure and the maximum value of center-of-mass collision energy. Recently, Schnier et al. demonstrated that the "effective temperatures" of protonated leucine enkephalin and doubly protonated bradykinin were similar when they were dissociated under the same SORI-CID conditions.[56] These experiments sampled a narrow range of "effective" temperatures between 200 and 350 °C. However, in the present study we found that the maximum temperature reached in the high-pressure experiment for protonated dialanine is 1390 K, whereas

Table 2. Average Internal Energies and "Effective" Temperatures Derived from MCA-CID Results

	⟨*E*⟩ , eV collision number		*T*, K collision number	
E_{CM}, eV	**5**	**15**	**5**	**15**
0.6	0.63 ± 0.02	0.89 ± 0.03	472 ± 9	557 ± 11
0.8	0.75 ± 0.02	1.09 ± 0.03	510 ± 10	620 ± 12
1.0	0.86 ± 0.03	1.28 ± 0.04	550 ± 11	680 ± 14
1.4	1.09 ± 0.03	1.65 ± 0.05	620 ± 12	790 ± 16
2.0	1.41 ± 0.04	2.18 ± 0.07	715 ± 14	930 ± 19
2.4	1.61 ± 0.05	2.50 ± 0.08	775 ± 16	1015 ± 20
3.0	1.90 ± 0.06	2.95 ± 0.09	855 ± 17	1125 ± 22
3.4	2.07 ± 0.06	3.23 ± 0.10	905 ± 18	1190 ± 24
4.0	2.33 ± 0.07	3.61 ± 0.11	970 ± 19	1270 ± 25
4.4	2.48 ± 0.07	3.83 ± 0.11	1010 ± 20	1320 ± 26
5.0	2.70 ± 0.08	4.14 ± 0.12	1060 ± 21	1390 ± 28

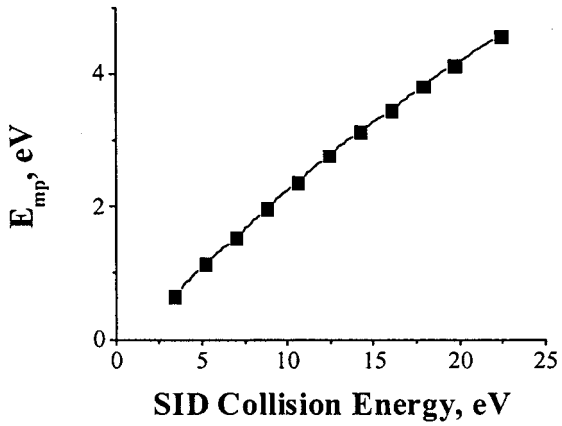

Figure 11. Most probable internal energy deposited by ion−surface impact.

the "effective" temperature of $C_{10}H_7Br^{+\bullet}$ obtained under the same experimental conditions was around 2000 K. The difference between the "effective" temperatures of bromonaphthalene and dialanine might be due to the difference in the fragmentation energetics. Obviously, the tightly bound ionic systems that require high internal excitation to dissociate can be heated to much higher temperatures than the ions that easily fragment at low internal excitation.

In accord with results obtained by us recently[23,24] the average energy for MCA-CID is not a linear function of the CM collision energy. In contrast, the most probable energy deposited upon SID rises almost linearly with the SID collision energy as shown in Figure 11. The observed difference between two excitation techniques was outlined earlier in this section and is probably due to deactivation of CID products by collisions with Ar.

The efficiency of kinetic-to-internal energy transfer can be derived from the slope of the plot presented in Figure 11. According to our results on average 21% of SID collision energy of protonated dialanine was converted into internal excitation. This value is consistent with previously reported conversion efficiencies on fluorinated SAM surfaces (18−28%) and lies above the range expected for alkanethiolate surfaces (12−17%).[41]

3. Dissociation Energetics and Mechanisms. The results summarized in Table 1 indicate that the lowest energy channels for the fragmentation of protonated dialanine correspond to the loss of CO (E_0 = 1.94 eV) and H_2O (E_0 = 1.92 eV). These reactions involve some structural rearrangements and therefore are characterized by relatively tight transition states. The formation of the $\mathbf{y_1}$ ion requires somewhat higher critical energy (E_0 = 2.06 eV) but is entropically more favored. The highest-energy channel for the primary fragmentation of Ala-AlaH$^+$ leading to the formation of the $\mathbf{a_1}$ ion has a critical energy of 2.11 eV and proceeds via a very loose TS with the activation entropy of about 10 eu. These results are in agreement with the results obtained by Klassen and Kebarle for single-collision CID of Gly-GlyH$^+$.[36] These authors have shown that the $\mathbf{y_1}$ ion has lower threshold energy, but that the $\mathbf{a_1}$ ion dominates at higher energies. This indicates that while the formation of $\mathbf{y_1}$ requires lower critical energy, it is characterized by a more tight transition state. Table 3 shows a comparison of the critical energies and activation entropies for the formation of immonium ion from GlyH$^+$ and Gly-GlyH$^+$ reported by Klassen and Kebarle, and AlaH$^+$ and Ala-AlaH$^+$ obtained in the present study. Although the critical energy for reaction 8 ($y_1 \rightarrow a_1$) derived from our modeling is characterized by a large uncertainty, it compares favorably with the critical energy for the fragmentation of GlyH$^+$. However, both the critical energies and activation entropies for the formation of immonium ion from Gly-GlyH$^+$ and Ala-AlaH$^+$ are significantly different.

Table 3. Comparison of the Present Results with Available Literature Data

precursor ion	fragment ion	E_0, eV	$\Delta S^{\ddagger}$, eu
(Gly-Gly)H$^+$	a_1 ($H_2NCH_2^+$)	1.89 ± 0.26	−3.2[a]
(Ala-Ala)H$^+$	a_1 (H_2NCHCH_3+)	2.11 ± 0.15[b]	9.8± 1.0[b]
GlyH$^+$	a_1 (H_2NCH_2+)	1.90 ± 0.07[a]	10.4[a]
AlaH$^+$ (y_1)	a_1 (H_2NCHCH_3+)	1.67 ± 0.35[b]	-

[a] CID threshold energies obtained by Klassen and Kebarle.[36] [b] Present work.

Scheme 3

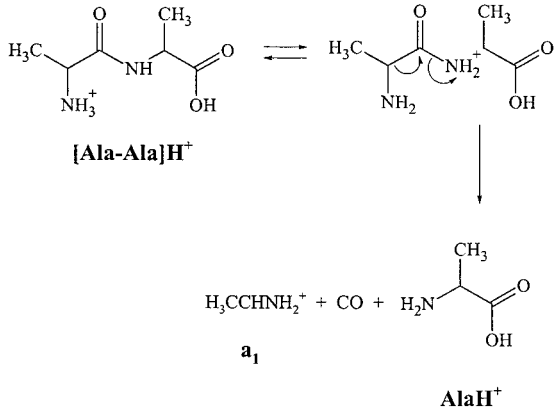

Formation of the $\mathbf{a_1}$ Ion from Ala-AlaH$^+$. Theoretical modeling involved in the interpretation of threshold experiments requires the knowledge of the mechanism of fragmentation to model the transition state structure. Klassen and Kebarle mentioned that the modeling of the transition state is one of the major sources of uncertainty in the threshold energies derived from their experiments. The relatively tight TS was obtained by these authors assuming that the immonium ion is formed from the unstable acylium $\mathbf{b_1}$ ion. Harrison and co-workers proposed that **b** ions have stable structures of protonated oxazolones.[57,58] Kinetic energy release measurements performed by this group indicated that the loss of CO from **b** ions proceeds in a stepwise fashion through the ring opening followed by the loss of CO from the unstable acylium configuration.[58,59] The resulting fragments are lower in energy than the reacting configuration that leads to a large kinetic energy release ($T_{1/2} \sim 0.5$ eV) associated with this reaction. However, small kinetic energy releases are associated with the formation of $\mathbf{a_1}$ ions from di- and tripeptides ($T_{1/2} \sim 0.05$ eV).[60] A simple mechanism shown in Scheme 3 accounts for these observations. This

mechanism assumes proton transfer from the energetically favored protonation site at the amine group[42] to the amide nitrogen in the first step followed by rupture of the amide and carbon−carbon bonds in the second step. A similar mechanism was proposed by Ambihapathy et al.[60] and Bouchoux et al.[61]We believe that the formation of $\mathbf{a_1}$ ions from both Gly-GlyH$^+$ and Ala-AlaH$^+$ proceeds via a loose transition state and the lower value for the critical energy obtained by Klassen and Kebarle is due to the energy−entropy tradeoff.

Loss of H_2O. Several groups studied dehydration of protonated peptides. Ballard and Gaskell studied the loss of water from protonated peptides using [^{18}O] labeling of the C-terminal carboxyl group.[62] They have shown that oxygen atoms from the C-terminal carboxylic acid group, side-chain hydroxyls, or peptide backbone can be involved in the dehydration process. Comparison of the fragmentation pathways of glycylglycine and its methyl ester derivative revealed that in the case of diglycine dehydration predominantly occurs from the C-terminus.[63] Gas-phase H/D exchange and CID studies provided evidence that the $\mathbf{b_2}$ ion formed by the loss of water from diglycine has the structure of protonated oxazolone.[55] Fragmentation of the $\mathbf{b_2}$ ion was characterized by the loss of CO, whereas the fragmentation of **b** ions formed by dehydration of larger polyglycines led to formation of nonsequence fragments. According to our observations the $\mathbf{b_2}$ ion formed from dialanine fragments predominantly by the loss of CO. Moreover, since only minor differences in the behavior of diglycine and dialanine can be expected, we believe that the $\mathbf{b_2}$ ion is formed from dialanine protonated at the hydroxyl oxygen and has the structure of protonated oxazolone.

Hoppilliard and co-workers have shown that protonation of the hydroxyl group of glycine requires 43 kcal/mol more energy than protonation of the amino group.[64] Klassen and Kebarle used low-level ab initio calculations to model the loss of water from glycine protonated at hydroxyl oxygen.[36] They found that lengthening the C−OH_2 bond led to a slight increase in energy with a maximum value of 1.4 kcal/mol at 2.4 Å. Further increase in bond length led to a drop in energy of 14 kcal/mol. The overall critical energy of 44.4 kcal/mol for the loss of water from glycine protonated at the N-terminus was estimated based on these calculations and confirmed by the threshold measurements.[36] This value is very close to the critical energy for the loss of water from Ala-AlaH$^+$ obtained in the present study (44.9 kcal/mol). Furthermore, the tight transition state associated with the formation of the $\mathbf{b_2}$ ion from dialanine confirms that the loss of water from Ala-AlaH$^+$ is characterized by a very similar mechanism.

Paizs et al. carried out ab initio calculations on the formation of $\mathbf{b_2}$ ions from peptides protonated at amide nitrogen.[65] According to these calculations the $\mathbf{b_2}$ ion is formed from the protonated peptide ion via a two-step process. In the first step the C−N bond rupture is followed by a closure of the oxazolone-type ring. The product of this step is an ion−molecule complex of protonated oxazolone and C-terminal amino acid or small neutral peptide molecule. The barrier for the formation of the ion−molecule complex is about 10 kcal/mol. Decomposition of this complex in the second step requires an additional 14 kcal/mol. The overall dissociation energy is around 20 kcal/mol and there is no reverse activation barrier for this reaction. Indeed, kinetic energy release measurements revealed that $\mathbf{b}_n$ ions are formed via a loose transition state (not for dehydration products).[58] However, we have shown earlier that the formation of the $\mathbf{b_2}$ ion from Ala-AlaH$^+$ by the loss of H_2O proceeds via a tight transition state. These observations show the influence of the site of protonation of peptide and the nature of the leaving group on the fragmentation mechanism. Similar to the formation of the $\mathbf{b_2}$ ion by the loss of C-terminal amino acid, its formation by water loss from dipeptide can proceed by the formation and decomposition of an ion−molecule complex. However, this complex is higher in energy than the dissociation products.

Scheme 4

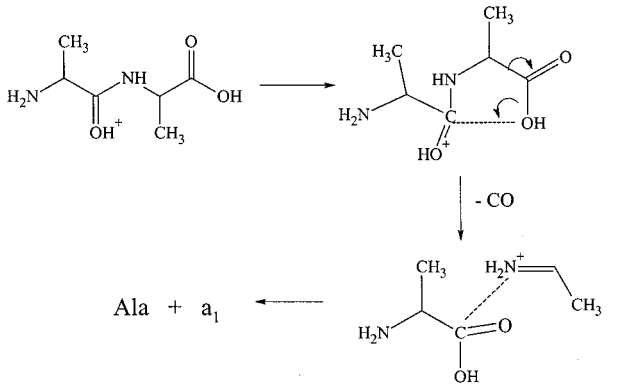

Loss of CO. Uggerud carried out ab initio calculations of the potential energy surface for protonated glycine and showed that loss of CO requires proton transfer to the carboxylic acid site followed by rearrangment.[66] This rearrangement proceeds via formation of a common intermediate structure by interaction of OH_2 with the nitrogen atom prior to fragmentation. A substantial reverse activation barrier is associated with the described rearrangement process.[66] The fragment ion formed by this mechanism is a weakly bound complex that readily dissociates to produce the immonium ion and water molecule. Assuming that CO loss from protonated dialanine occurs via a similar pathway, one would expect to observe subsequent loss of H_2O from *m*/*z* 133 to yield the a_2 ion. However, as mentioned earlier, double resonance experiments have shown no evidence for water loss from *m*/*z* 133. Thus a different pathway should be considered for the loss of CO from Ala-AlaH$^+$.

Scheme 4 shows a plausible pathway for CO loss from protonated dialanine. Ab initio calculations performed by Cassady and co-workers[68] indicated that the most favorable protonation site of diglycine is the amino nitrogen. However, protonation at the amide carbonyl oxygen requires only 1.69 kcal/mol more energy. Since the relative protonation energetics for diglycine and dialanine are expected to be similar, we assumed that proton transfer to the amide carbonyl oxygen is very fast and used the latter structure as a starting point in Scheme 4. The mechanism is based on nucleophilic attack of acyl carbon by hydroxyl that results in a loss of CO from the protonated parent ion in a first step. It is clearly seen that stabilization of the fragment ion formed in this step cannot occur via loss of water. Rather it requires proton transfer to the amide nitrogen followed by a cleavage of amide bond and formation of neutral alanine and internal immonium ion.

(61) Bouchoux, G.; Bourcier, S.; Hoppilliard, Y.; Mauriac, C. *Org. Mass Spectrom.* **1993**, *28*, 1064.
(62) Ballard, K. D.; Gaskell, S. J. *J. Am. Soc. Mass Spectrom.* **1993**, *4*, 477.
(63) Reid, G. A.; Simpson, R. J.; O'Hair, R. A. J. *J. Am. Soc. Mass Spectrom.* **1998**, *9*, 945.
(64) Bouchonnet, S.; Hoppilliard, Y. *Org. Mass Spectrom.* **1992**, *27*, 71.
(65) Paizs, B.; Lendway, G.; Vékey, K.; Suhai, S. *Rapid Commun. Mass Spectrom.* **1999**, *13*, 525.
(66) Uggerud, E. *Theor. Chim. Acta* **1997**, *97*, 313.
(67) Fang, D.-C.; Yalcin, T.; Tang, T.-H.; Fu, X.-Y.; Harrison, A. G.; Csizmadia, I. G. *J. Mol. Structure (THEOCHEM)* **1999**, *468*, 135.
(68) Zhang, K.; Zimmerman, D. M.; Chung-Phillips, A.; Cassady, C. J. *J. Am. Chem. Soc.* **1993**, *115*, 10812.

Dissociation of the b_2 Ion. The critical energy for the dissociation of the $\mathbf{b_2}$ ion ($\mathbf{b_2} \rightarrow \mathbf{a_2} + CO$) obtained from our modeling is 0.98 eV. Yalcin et al. reported a somewhat higher critical energy of 1.49 eV for this reaction based on ab initio calculations.[58] However, the critical energy for the formation of the $\mathbf{a_2}$ ion from the $\mathbf{b_2}$ ion of 25.6 kcal/mol (1.11 eV) was obtained in a more recent ab initio study by Fang et al.[67] The critical energy for reaction 5 obtained from our modeling is in close agreement with the predictions from the ab initio calculations.

Conclusions

We have performed a detailed investigation of the dissociation of protonated dialanine using multiple-collision CID and SID techniques. The energetics and dynamics of the four primary and some secondary fragmentation pathways were determined from the RRKM modeling of the collision energy-resolved fragmentation efficiency curves. The results obtained from both experiments could be modeled using very similar RRKM parameters. Moreover, the same analytical form for the energy deposition function was used to model SID and MCA-CID results. We have previously shown that the proposed form for the EDF can be used to reproduce both the single-collision and multiple-collision CID results. In the present study for the first time we apply the same ideas to reproduce the results of SID experiments.

Implementation of both multiple-collision activation (MCA-CID) and SID on the same instrument allowed us to perform a direct comparison between these excitation techniques. The comparison was performed by converting the SID energy scale into the center-of-mass frame. The best overlap between the SID and MCA-CID results was obtained with the assumed mass of the neutral encounter of 46 amu. We demonstrated that the energy-resolved fragmentation efficiency curves obtained for the high-pressure MCA-CID and SID were very alike. The correspondence between the fragmentation efficiencies clearly demonstrates that the internal energy distributions of dialanine activated by multiple collisions and by surface impact are very similar. Indeed, our modeling results showed that the internal energy distributions of the precursor ion activated by multiple collisions and by ion−surface impact were very comparable. The differences between the SID and MCA-CID energy deposition function probably arise from collisional deactivation of ions in MCA-CID experiments that do not occur in the SID experiments. Further studies are required to gain a detailed understanding of the similarities and differences between SID and high-pressure multiple-collision CID. However, in the present study we have demonstrated a remarkable similarity between these techniques. We have shown that the ion excitation upon ion−surface collisions proceeds via multiple interactions of the projectile ion with chemical groups on the surface that essentially lead to thermalization of the ion's internal degrees of freedom. The mean internal energy deposited by SID rises almost linearly with the collision energy at least in the range of collision energies sampled in the present study. We found that about 21% of the initial collision energy was transferred into the internal modes of the projectile ion.

The lowest energy dissociation channels correspond to the loss of H_2O and CO from the precursor ion. These reactions are associated with relatively tight transition states indicating that they involve some rearrangement steps. The loss of water from Ala-AlaH$^+$ has very similar energy and entropy requirements as the water loss from protonated glycine. The formation of the $\mathbf{y_1}$ and $\mathbf{a_1}$ ions requires higher critical energies. However, these reactions are more entropically favored than the loss of water and CO. The $\mathbf{a_1}$ ion dominates in the mass spectrum because of the very loose transition state associated with its formation. The loose transition state for the formation of the immonium ion confirms that this reaction does not proceed via a stepwise mechanism where the immonium ion is formed by the loss of CO from the unstable acylium $\mathbf{b_1}$ ion. The concerted mechanism proposed by Ambihapathy et al.[60] will, probably, lead to higher activation entropy for this reaction. Comparison of the breakdown curves calculated for the characteristic time of the FT-ICR experiment (5 s) and a short time scale of a triple quadrupole mass spectrometer (20 μs) revealed that the intensities of the ions corresponding to the loss of H_2O ($\mathbf{b_2}$ ion) and CO from the precursor ion are strongly depleted on a microsecond time scale. Thus it is not surprising that these fragments are not commonly observed using short time scale mass spectrometers.

In the present study we have demonstrated that the modeling approach proposed by us previously can be successfully applied to study fragmentation energetics of small peptides. Further studies are necessary to perform a more thorough comparison of SID and MCA-CID and obtain a more detailed understanding of the energetics and dynamics of peptide fragmentation.

Acknowledgment. This research was supported by NSF grants CHE-9616711 and CHE-9634238 and by DOE grant DE-FG02-97ER14813.

JA001384W